Supplementary information for: Functional patterned multiphoton excitation deep inside scattering tissue

Eirini Papagiakoumou, Aurélien Bègue, Ben Leshem, Osip Schwartz, Brandon Stell, Jonathan Bradley, Dan Oron and Valentina Emiliani

Numerical simulations

For the numerical simulation of the evolution of temporally focused beams inside turbid tissue, we used 100 fs pulses centered at either 800 nm or 950 nm. As a scattering sample we considered a homogeneous medium of randomly distributed dielectric spheres of 2 μm, having a refractive index higher by 0.1 than the surrounding medium and a concentration of 1 scatterer per 1000 μm^3. The simulations were performed iteratively, whereby in each simulation step the beam was propagated via the angular spectrum of plane waves approach, and then a spatial phase was imprinted on it according to the distribution of scattering spheres. This approach, where backscattering was neglected, was a legitimate approximation within brain slices, where the index contrast within the sample was typically very small. To ensure that the results are insensitive to the particular choice of the refractive index contrast, we have performed additional simulations for spheres having a refractive index higher by 0.05 and 0.025 than the surrounding medium and an average concentration of 4 and 16 scatterers per 1000 μm^3 respectively, leading to a similar scattering length. The range of index mismatch chosen is in accordance with values that can be found in literature for rat cortical brain slices[1,2]. As seen in Fig. S1, all three

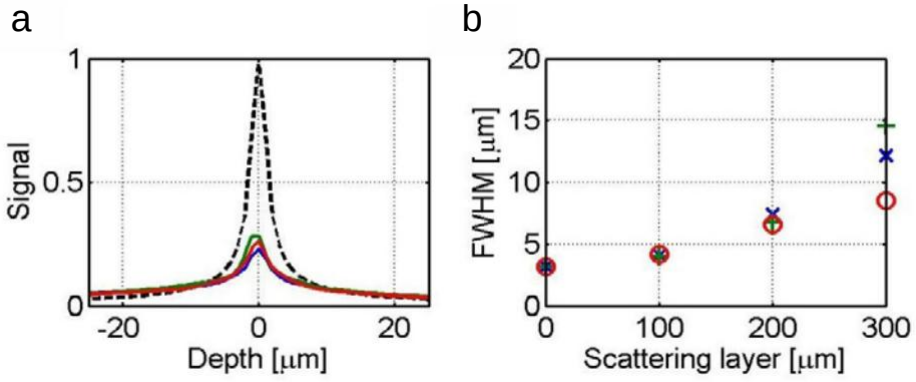

Figure S1: **a**, Simulated axial response of the two-photon signal after propagation through 200 μm of scattering medium for realizations with similar scattering length but different index contrast (0.1 blue, 0.05 green, 0.025 red, no scattering dashed black line). **b**, Full width at half maximum of the axial responses simulated in (**a**) for different medium thicknesses.

configurations lead to a similar axial response, pointing to the fact that the important parameter is the scattering length.

Quantification of transmitted image quality

Without scattering, the GPC patterns have nearly uniform intensity. Propagation leads to two effects: speckle formation and pattern distortion. To characterize speckle formation we used two different measures. The first is a rough non-uniformity and the second is a calculation of speckle contrast for a 'statistical ensemble' of 100 images in experiment and 1000 images in numerical calculations. The non-uniformity (NU) is calculated as follows: The outline of the illumination shape is obtained by thresholding. Then, the excitation non-uniformity is defined as the standard deviation of the measured intensity normalized to the mean intensity within the shape outline:

$$NU = \left(\overline{I(x,y)^2} - \overline{I(x,y)}^2 \right)^{\frac{1}{2}} \Big/ \overline{I(x,y)}$$

For no distortion NU=0. Here the upper score denotes an average over the (x,y) coordinates of a single image within the region of interest defined by the thresholding.

To characterize pattern distortion, P, we compute the intensity cross-correlation within a region of interest A containing the excitation shape:

$$P = \iint_{dA} I_d(x,y) I_s(x,y) \Big/ \sqrt{\iint_{dA} I_d(x,y)^2 \iint_{dA} I_s(x,y)^2}$$

Where I_d is the desired intensity pattern (without scattering) and I_s is the measured (simulated) one. For no distortion P=1.

These measures of NU and P are given in Table 1 for the cases given in the manuscript.

	Non-uniformity (NU)	Pattern distortion (P)
Gaussian (sim)	0.66 (2.36)	0.94 (0.45)
Gaussian (exp)	0.36 (0.97)	0.97 (0.84)
Circular spot (exp)	0.22 (0.76)	0.98 (0.80)
Neuron (exp)	0.36 (0.59)	0.99 (0.81)
Acute neuron (550μm)	0.38 (0.89)	0.98 (0.62)

Table 1: Analysis of image quality after scattering samples. Values with (without) temporal focusing are given for all cases shown in the manuscript.

Speckle contrast over an 'ensemble average'.

One image on its own does not contain enough information for statistical calculations (as reflected in the small number of speckles within one image). To evaluate the non-uniformity through a large number of realizations and for different beam sizes, we calculated and measured the 'ensemble average' speckle contrast, SC, defined as:

$$SC = \left(\left\langle I(x,y)^2 \right\rangle - \left\langle I(x,y) \right\rangle^2 \right)^{\frac{1}{2}} \Big/ \left\langle I(x,y) \right\rangle$$

Here the brackets denote an 'ensemble average' over 1000 images (in numeric simulation), where each image is obtained with different statistical realization of the scattering medium, or 100 images (in experiments).

Numerical simulations were carried for homogeneous medium of randomly distributed dielectric spheres of 2 μm, having a refractive index higher by 0.3 than the surrounding medium and a concentration of 1 scatterer per 2000 μm^3 (the refractive index was chosen to match this of the latex beads used in the experiment described below, the rest of the parameters were chosen so that the scattering length will be similar to that of brain tissue). The medium thickness was 200 μm and the beam sizes were 10 μm-30 μm in intervals of 5 μm.

Experimental generation of different realizations of a scattering medium was achieved by using a latex beads solution as a phantom. Images were captured for 50 ms every 1.2 seconds using an EMCCD camera (Andor Luca) and a mechanical shutter, so that the beads were randomly redistributed between the frames due to diffusion. The temporal focusing setup was similar to the one described below.

The solution of latex beads, used as a phantom scattering medium, contained 0.5% CTAB, 20% glucose and 1:2000 μm^3 surfactant free amine aliphatic latex beads of diameter 2.1 μm.

In this manner a 'statistical ensemble' of 100 images was constituted for each beam size. The beam sizes measured were 10, 20 and 30 μm.

The time interval of 1.2 seconds was based on experimental measurements performed without temporal focusing. For short intervals between frames the degree of correlation between consecutive images was high, and dropped as the time interval was extended, finally reaching a plateau (corresponding to full redistribution of the scatterers by diffusion) after about 1.1 seconds. Then, for the chosen time interval of 1.2 seconds, we made sure that upon summation of multiple consecutive images, the overall contrast decreased inversely with the square of the

number of summed images (the experimental value was a power law with an exponent of -0.46). Both measurements confirm that indeed every frame is statistically independent of the preceding one. The results have been summarized in Fig. 2c.

Correlation between speckle patterns of 'neighboring' colors.

Correlation of speckle patterns between 'neighboring' colors is responsible for the extra smoothing of the excitation patterns along the axis where colors are angularly dispersed. This effect is closely related to a smoothing mechanism often used in direct drive fusion experiments, termed 'Smoothing by Spectral Dispersion' (SSD)3. To show this, we plot in Fig. S3 simulated speckle patterns for several frequency components, each spaced about 5% of the excitation bandwidth from one another. 'Motion' of speckles towards the right is apparent going from lower frequencies (Fig. S3a) to higher frequencies (Fig. S3d). This is also exemplified in Figure S4, where vertical and lateral cross-correlation patterns are shown for neighboring colors. The autocorrelation trace of the speckle pattern (Fig. S4a) shows a sharp peak of the speckle size on top of a broad peak, corresponding to the illumination size. The cross-correlation for increasing frequency separation (Fig. S4b-d) show high correlation at a shifted position for the lateral cross-correlation curves (red) and reduced correlation, centered at an unshifted position for the vertical direction (blue).

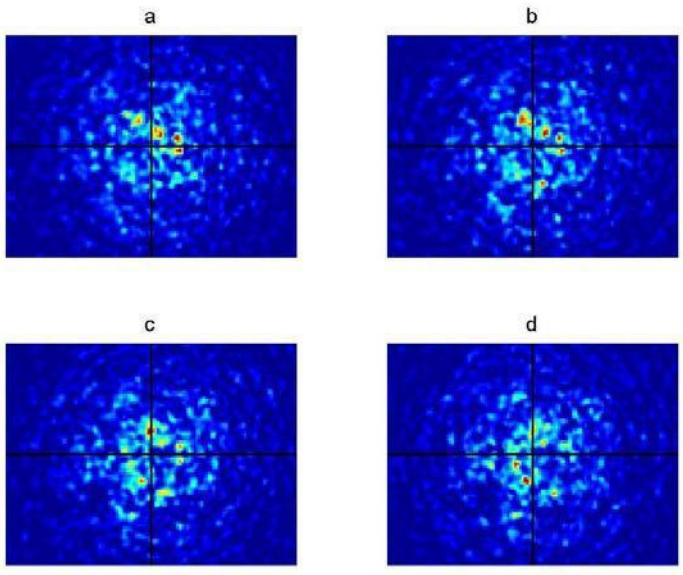

Figure S3: Simulated speckle patterns for four different excitation colors, each shifted by about 5% of the excitation pulse spectral bandwidth from one another, at the temporal focal plane. Close inspection reveals that speckles in consecutive images are correlated and shifted to the right by about 1 μm per image.

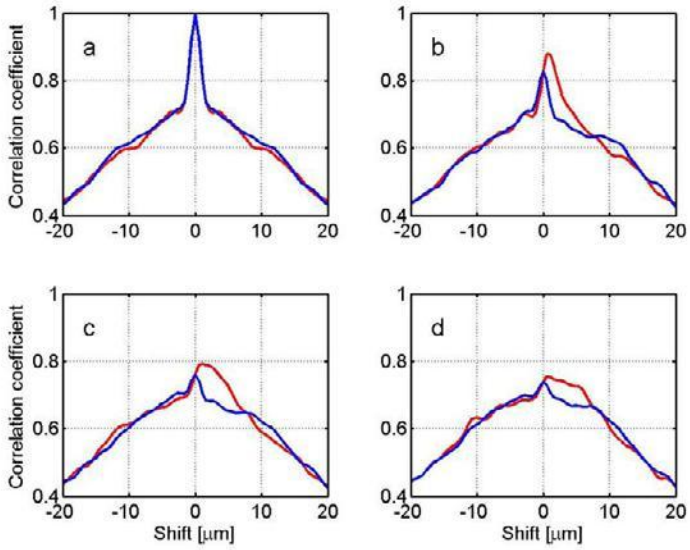

Figure S4: Intensity cross-correlations between speckle patterns of 'neighboring' colors with temporal focusing. The intensity autocorrelation for a given color (**a**) is similar for vertical shifts (blue) and for horizontal shifts, along the direction of dispersion (red), and peaks at zero shift. For 'neighboring' (**b**,**c**,**d**, each shifted by about 5% of the excitation pulse spectral bandwidth from one another) colors the cross-correlation peak rapidly decays to the overall Gaussian background in the vertical direction, but persists and peaks at positive shifts for the horizontal ones, indicating a horizontal shift of the speckle pattern, and leading to significant smoothing along it.

Scattering length of fixed slices.

The scattering length of the fixed coronal cortical slices was estimated by measuring the 2P excited fluorescence signal on a rhodamine-6G coverslip after going through several slice thicknesses. Measurements were performed by using a circular 15-µm diameter spot as the excitation pattern and by integrating the fluorescence signal in the area of the spot.

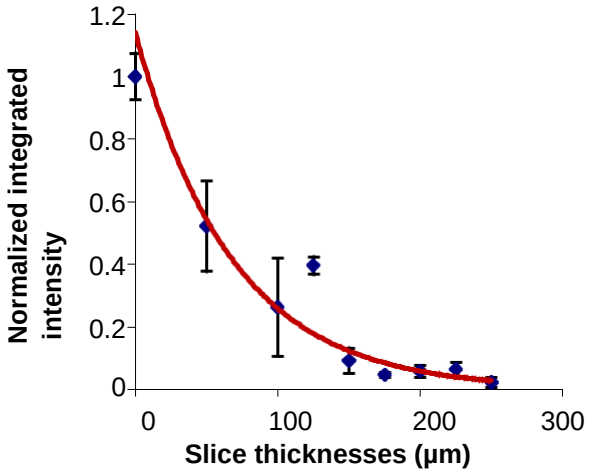

Figure S5: Integrated 2P excited fluorescence signal *vs* slice thickness. The scattering length, ℓ_s , was deduced by fitting the experimental data with an exponential decay (red curve) and in this case found to be 135±12 µm.

Supplementary Methods

Optical setup for beam propagation characterization

The characterization of the beam propagation through the different types of brain slices was done in a microscope configuration with two opposite placed objectives (shown in Fig. 2b of the main article), as described in our previous work 2P fluorescence was excited through a 60x microscope objective (Olympus, LUMPLFL60xW/IR2, NA 0.90) on a ~1 μm-thick fluorescent layer of rhodamine-6G in PMMA, spin-coated on a glass coverslip, through different thicknesses of fixed or acute brain slices. The emitted fluorescence was collected by a second objective (Olympus, UPLSAPO60xW, NA 1.20) placed opposite to the excitation one, disposing a correction collar for the coverslip thickness. The imaging objective was fixed and focused on the thin fluorescent layer, while the upper one was moved along the axial direction (±40 μm around its focal plane, in steps of 0.5 μm) with a piezo-scanning stage working in closed-loop (MIPOS100SG, Piezosystem Jena). Fluorescence was imaged by a collection tube lens (f=150 mm) to a CCD camera (CoolSNAP HQ2, Roper Scientific). To reject the excitation light, an emission filter (Chroma Technology HQ 535/50M) and a dichroic filter (Chroma Technology 640DCSPXR) were placed in front of the CCD camera.

To deduce the axial resolution, we scanned the excitation objective through the fluorescent layer and measured the excited fluorescence intensity at each plane. For each plane, the integrated intensity over a region of interest equal to the contour-line of the excitation shape in the focal plane was measured. The corresponding values of the integrated intensities as a function of the axial position were plotted and the FWHM of the curve was taken as the value for the axial resolution

Temporal focusing setup. The accordingly modulated laser beam for the generation of the low-NA Gaussian beam or GPC patterns was sent to a reflectance diffraction grating (830 lines/mm) aligned perpendicular to the optical axis of the microscope. The illumination angle of the grating was 42º at 800 nm, or 52° at 950 nm, such that the +1 order diffracted beam at the center frequency of the excitation pulse was directed along the optical axis of the microscope. The grating dispersed the various frequency components of the beam, which were imaged onto the sample via a telescope comprised of an achromatic lens (f=500mm) and the excitation objective. Whenever experiments without temporal focusing were performed, the diffraction grating of the optical setup was replaced with a plane dielectric mirror.

Gaussian beam illumination. The laser beam was spatially expanded with a variable beam expander (2x-5x) and sent to the diffraction grating for TF. The expansion of the laser beam

before the grating was such as the lateral size of the Gaussian beam at the sample plane was 11 μm at FWHM.

Generalized Phase Contrast beam illumination. In GPC the output light distribution is obtained by the interference between a signal and an unscattered light component (zero order), which travel along the same optical axis. The desired target intensity map is converted into a spatially similar phase map that in our case was addressed on a Liquid crystal on Silicon Spatial Light Modulator (LCOS-SLM). A phase contrast filter (PCF) placed at the Fourier plane of the SLM imposes a half-wave (λ/2) phase retardation between the on-axis focused component and the higher-order diffracted Fourier components. The interference between the phase-shifted focused and the scattered light, allows generating a pure phase-to-intensity conversion at the output plane. In the experimental realization (schematic layout in Fig. S6) the LCOS-SLM was controlled by custom-designed software that, given a target intensity distribution at the focal plane of the microscope objective, converts the intensity map into a binary phase map and addresses the

output profile to the SLM. The beam reflected from the SLM was separated in its Fourier components by a 400 mm focal length achromatic lens and focused on the PCF, positioned at the Fourier plane of this lens. The on-axis, low spatial frequency components were shifted in phase by λ/2, by the PCF and then, the second 300 mm achromatic lens recombined the high (signal wave) and low (synthetic reference wave) spatial frequency components. The introduced phase shift caused these components to interfere and produced an intensity distribution according to the spatial phase information carried by the higher spatial frequencies. Then the beam was sent to the diffraction grating and the setup for temporal focusing was following. The 500 mm lens and the microscope objective formed the second 4-f lens system that scaled the intensity distribution (~ 1/110) on the sample plane.

For further details on how to get optimal contrast conditions at the output plane of the system (focal plane of the 300 mm lens, which coincides with the grating plane) and how to choose the size of the PCF, the reader can refer to our previous work.

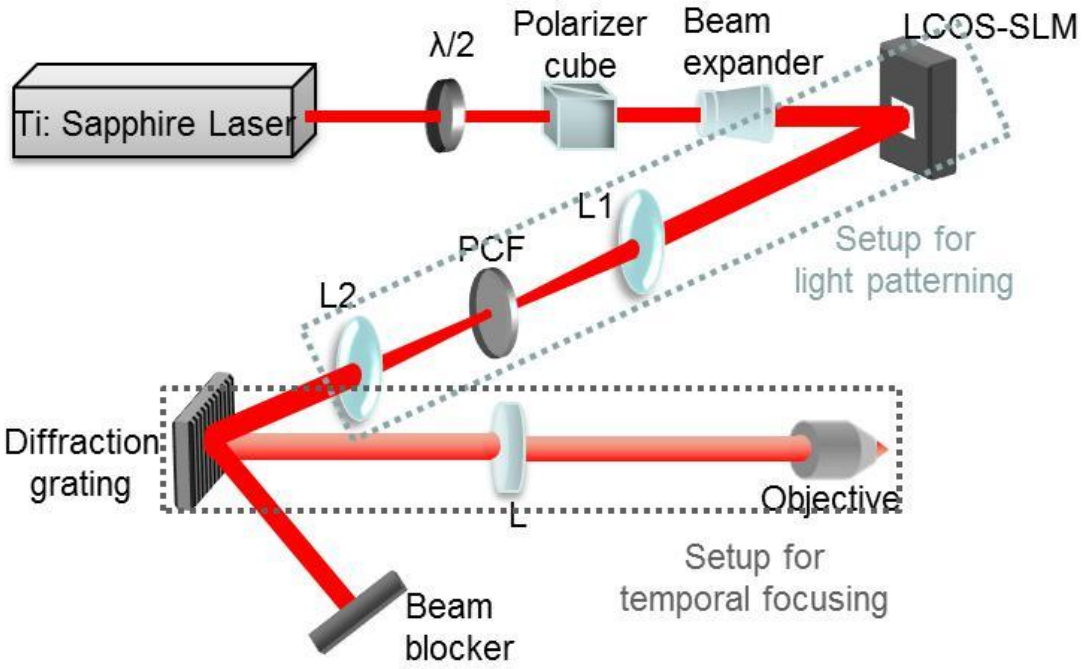

Figure S6: Layout of the optical setup for GPC (Beam expander: 10×, LCOS-SLM: Liquid Crystal on Silicon Spatial Light Modulator, L1, L2, L: lenses with focal lengths f_1 = 400 mm, f_2 = 300 mm and f = 500 mm, PCF: Phase Contrast Filter, Diffraction Grating: 830 lines/mm).

References

1. Roper, S.N., et al. In vivo detection of experimentally induced cortical dysgenesis in the adult rat neocortex using optical coherence tomography. *J Neurosci Methods* **80**, 91-98 (1998).
2. Binding, J., et al. Brain refractive index measured in vivo with high-NA defocus-corrected full-field OCT and consequences for two-photon microscopy. *Opt Express* **19**, 4833-4847 (2011).
3. Skupsky, S., et al. Improved Laser-Beam Uniformity Using the Angular-Dispersion of Frequency-Modulated Light. *J Appl Phys* **66**, 3456-3462 (1989).